Supporting Information

Destruction of Opportunistic Pathogens via Polymer Nanoparticle-Mediated Release of Plant-Based Antimicrobial Payloads

Dahlia N. Amato,[a] Douglas V. Amato,[a] Olga V. Mavrodi,[b] Dwaine A. Braasch,[a] Susan E. Walley,[a] Jessica R. Douglas,[a] Dmitri V. Mavrodi,[b] and Derek L. Patton[a]**

Table S1. General formulation of organic stock solutions for thiol-ene photopolymerization in miniemulsion.

Organic Components	Mass [g]	Moles [mmol]	wt. %
Diallyl phthalate	2.57	10.44	23.53
GDMP	2.00	8.39	18.32
PETMP	0.50	1.02	4.58
Carvacrol	2.90	19.31	26.56
p-methoxyphenol	0.05	0.40	0.46
Irgacure 184	0.10	0.49	0.92
Hexadecane	0.60	2.65	5.49
Thymol	2.20	14.65	20.15

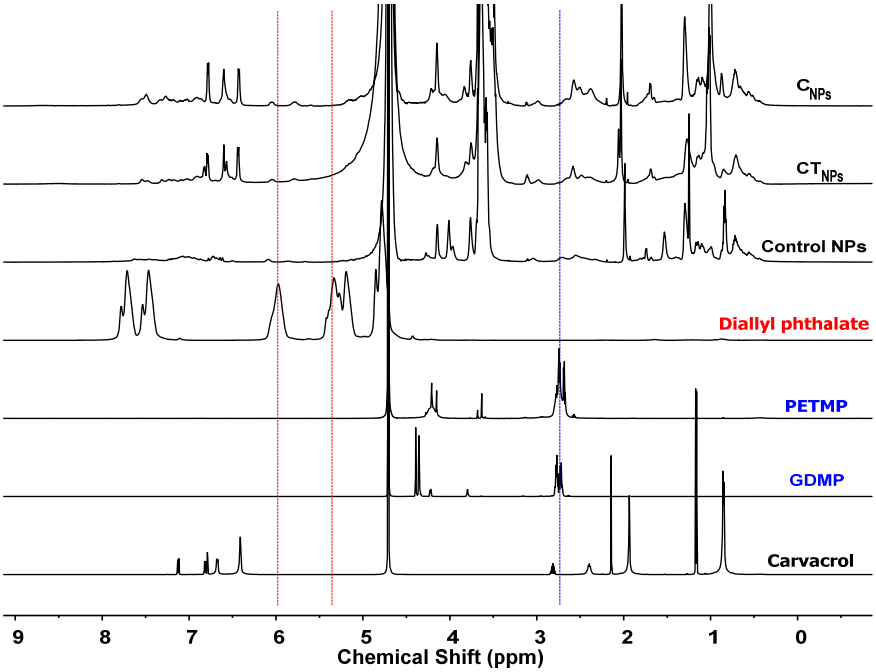

Figure S1. ^{1}H NMR of the starting materials: diallyl phthalate, PETMP, GDMP, carvacrol, and all three types of NPs after UV polymerization. ^{1}H spectrum confirmed the disappearance of both mercaptopriopionate (2.62-2.83 ppm) and alkene (5.07-5.45 ppm and 5.87-6.10 ppm) peaks after UV exposure.

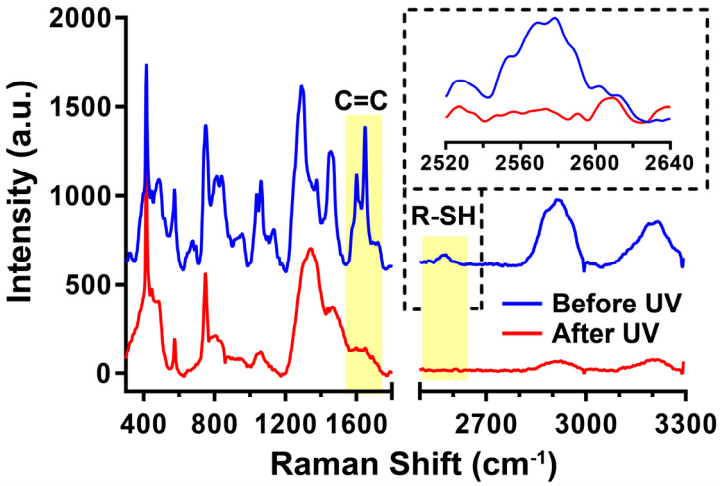

Figure S2. Raman spectra of TC_{NPs} after ultrasonication (top, blue) and after exposure to UV light (λ_{365} nm) (bottom, red).

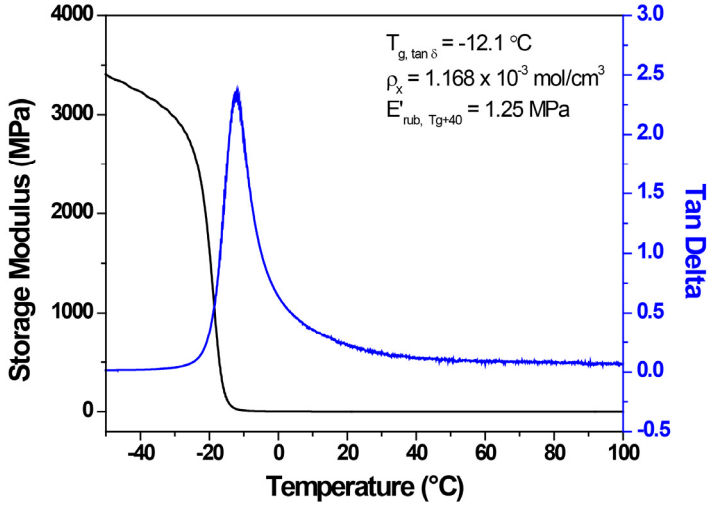

Figure S3. Plots of storage modulus vs temperature and tan δ vs temperature of the GDMP+PETMP+diallyl phthalate base resin prepared in the absence of small molecules (i.e. thymol, carvacrol, heaxadecane, etc.) and polymerizable surfactant. These data were only used to approximate the thermomechanical properties and crosslink density that may be expected for the polythioether nanoparticles.

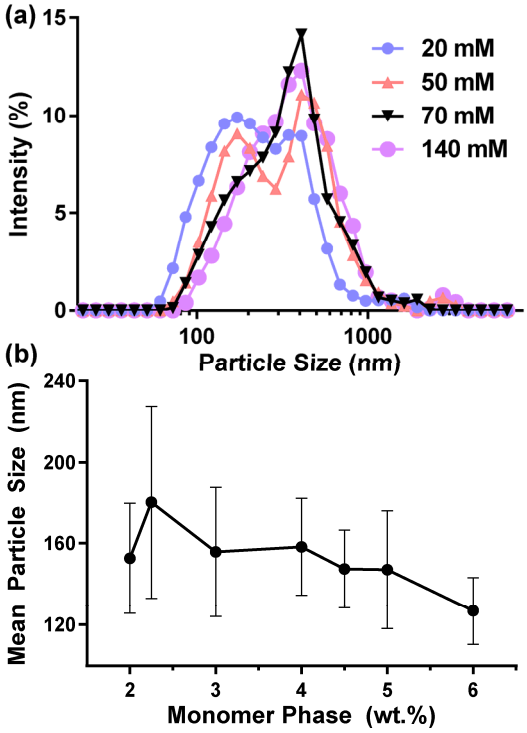

Figure S4. A) Surfactant concentration sweep of Hitenol BC-20 and B) Effect of weight fraction of the organic monomer phase on particle size for TC_{NPs}.

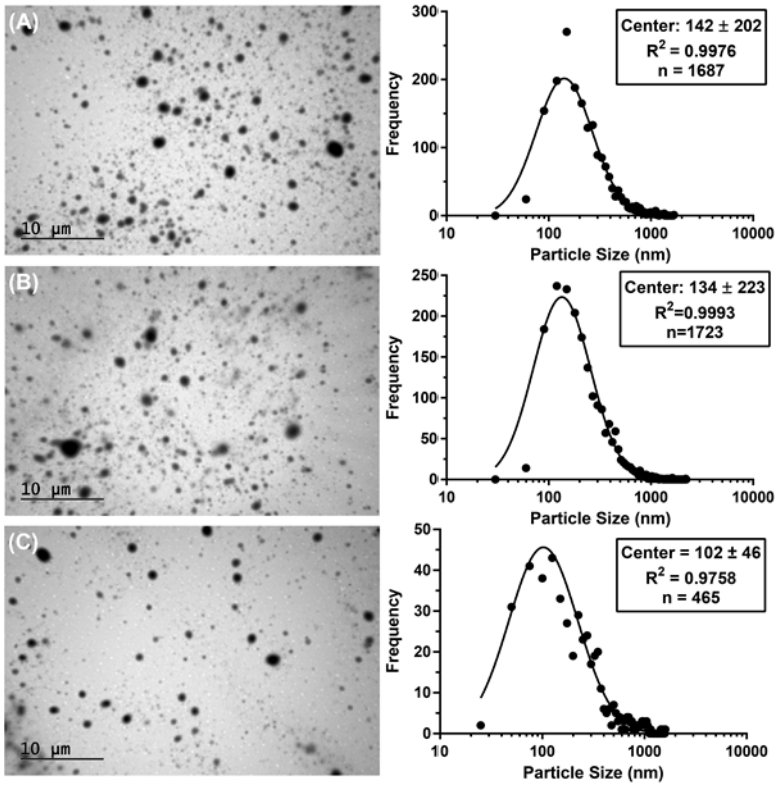

Figure S5. Transmission electron microscopy and particle of (A) control NPs, (B) C_{NPs}, and (C) TC_{NPs}.

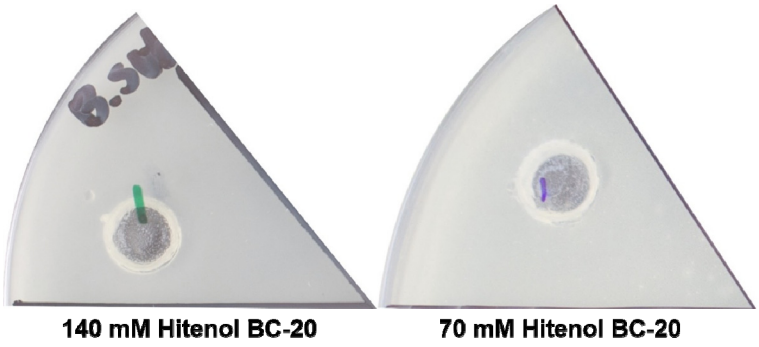

Figure S6. Absence of antimicrobial activity of *B. subtilis* by Hitenol BC-20 at 140 and 70 mM.

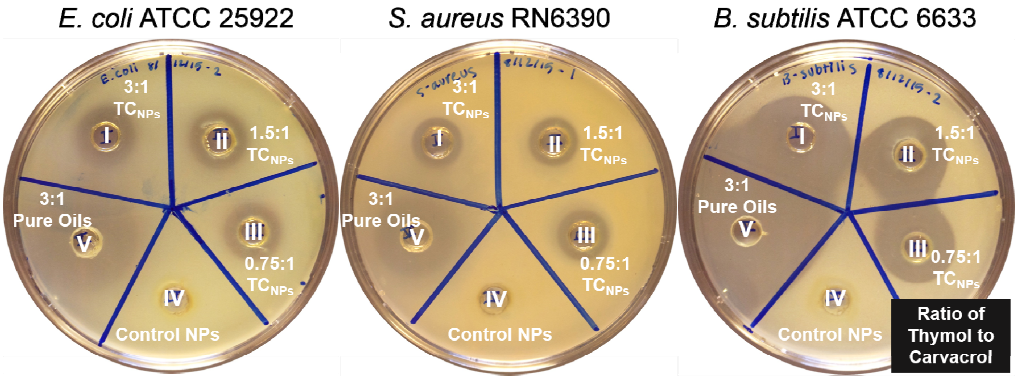

Figure S7. Antimicrobial activity of nanoparticles loaded with different ratios of carvacrol and thymol (treatments I, II, and III). Controls included empty NPs (IV) and a 12:4 mixture of pure carvacrol and thymol (V).

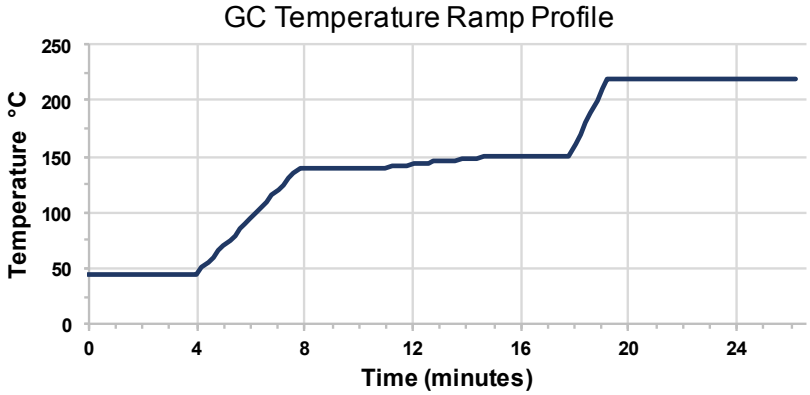

Figure S8. Ramping conditions used for GC-MS separation of thymol and carvacrol isomers.

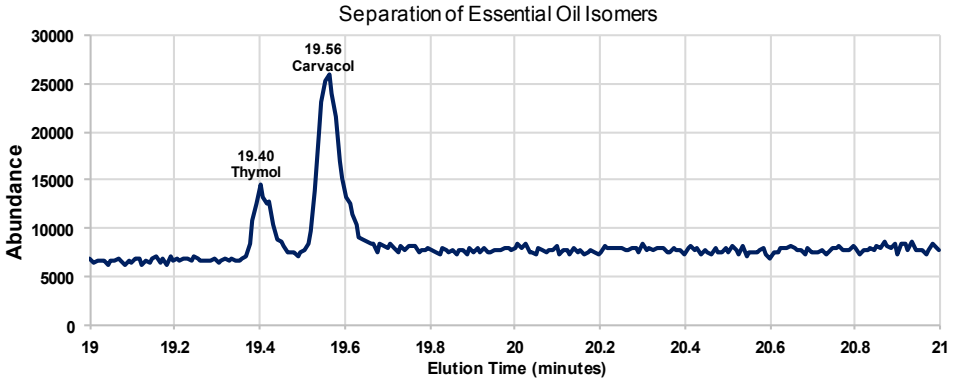

Figure S9. Example separation of thymol and carvacol isomers eluting at 19.40 and 19.56 min respectively.

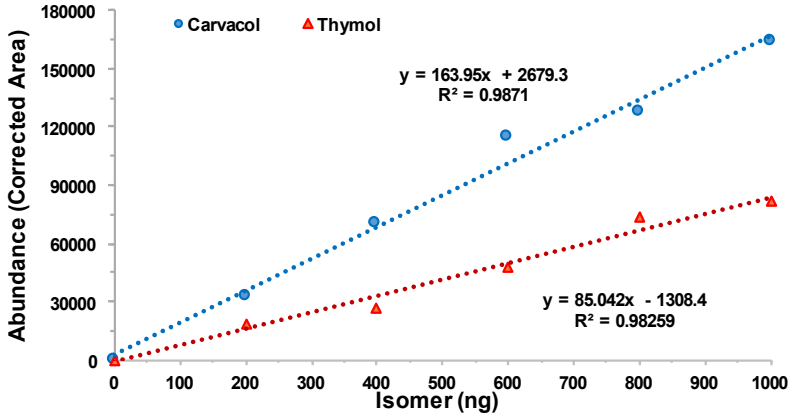

Figure S10. Calibration curves for thymol and carvacrol isomers.

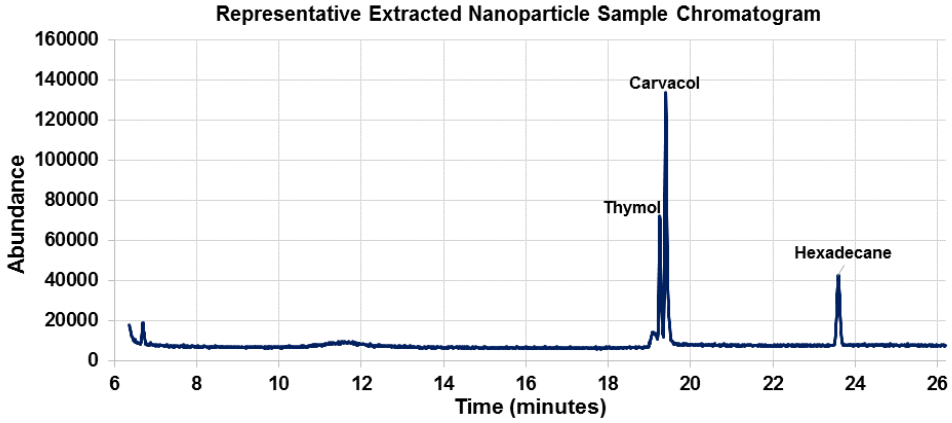

Figure S11. A representative chromatogram of extracted nanoparticles depicting the elution of thymol, carvacol and hexadecane.

Table S2. Nanoparticle size and concentration for different formulations.

Sample	Particle size (nm)	[NP] (particles mL^{-1})
Control NPs (Butyl acetate)	183 ± 19	1.4×10^{13}
C_{NPs} (Carvacrol)	148 ± 24	2.7×10^{13}
TC_{NPs} (Thymol and Carvacrol)	147 ± 19	2.7×10^{13}

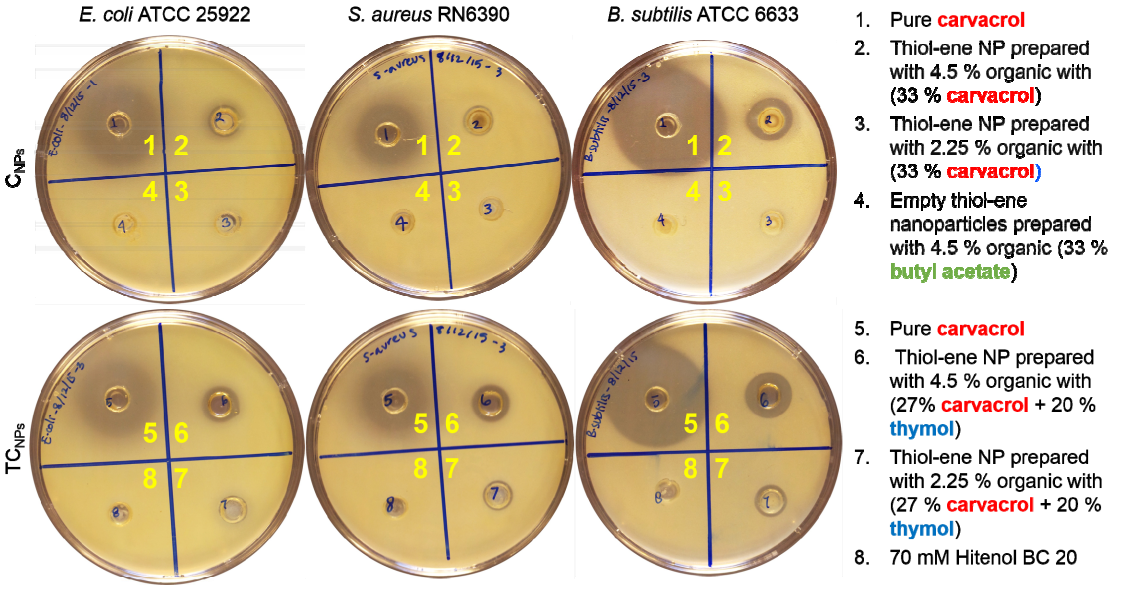

Figure S12. Additional data with controls: inhibition of *B. subtilis* ATCC 6633, *E. coli* ATCC 25922, and *S. aureus* RN6390 with thiol-ene nanoparticles containing different ratios of essential oils (shown in Table S5).

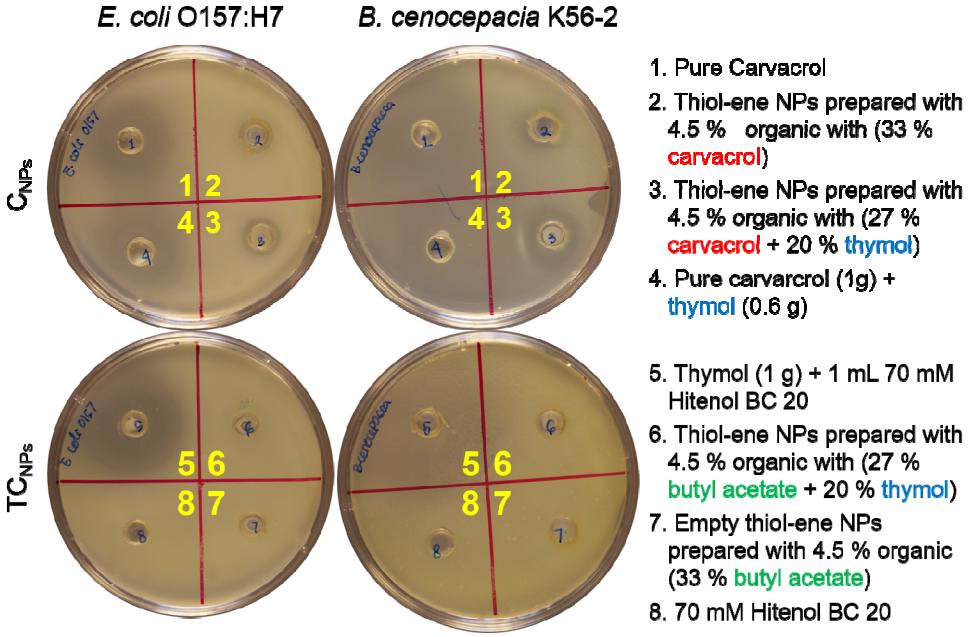

Figure S13. Additional data with controls: Inhibition of *E. coli* O157:H7 and *B. cenocepacia* K56-2 with different types of NPs.

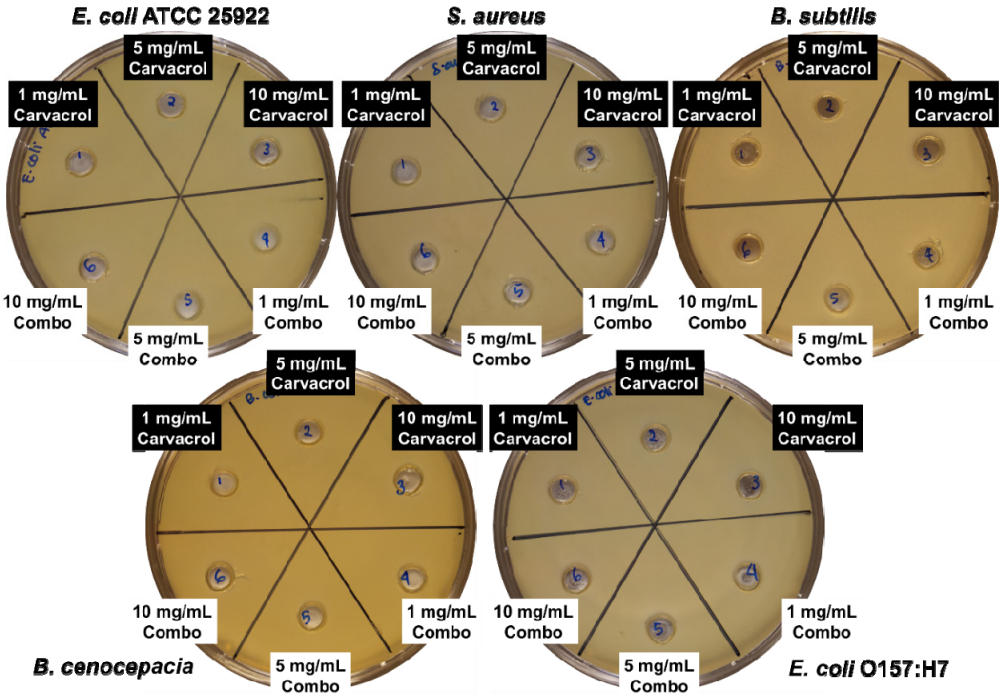

Figure S14. Absence of antimicrobial activity for different concentrations of carvacrol and thymol/carvacrol in 70 mM Hitenol BC-20.

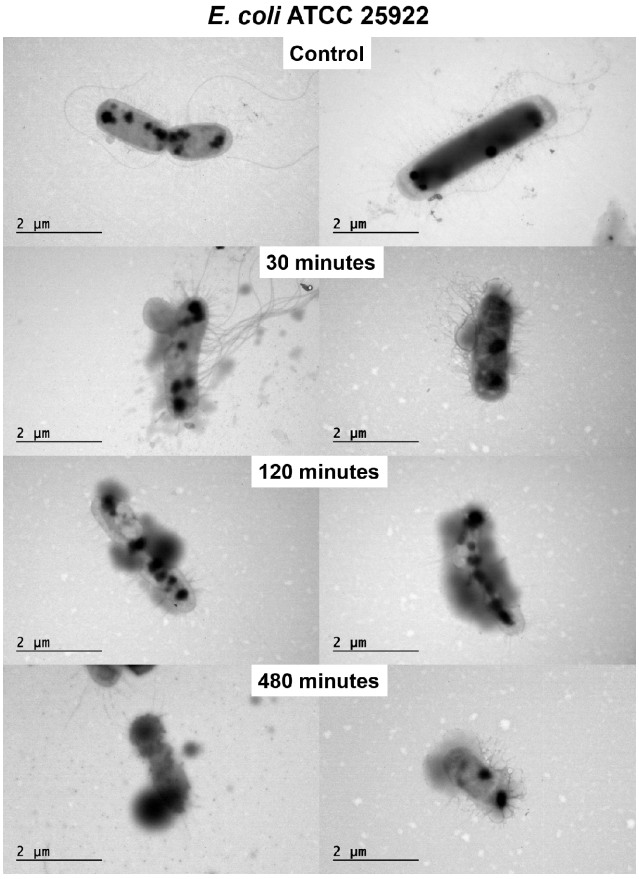

Figure S15. Additional TEM images of *E. coli* ATCC 25922 with TC_{NPs} over time.

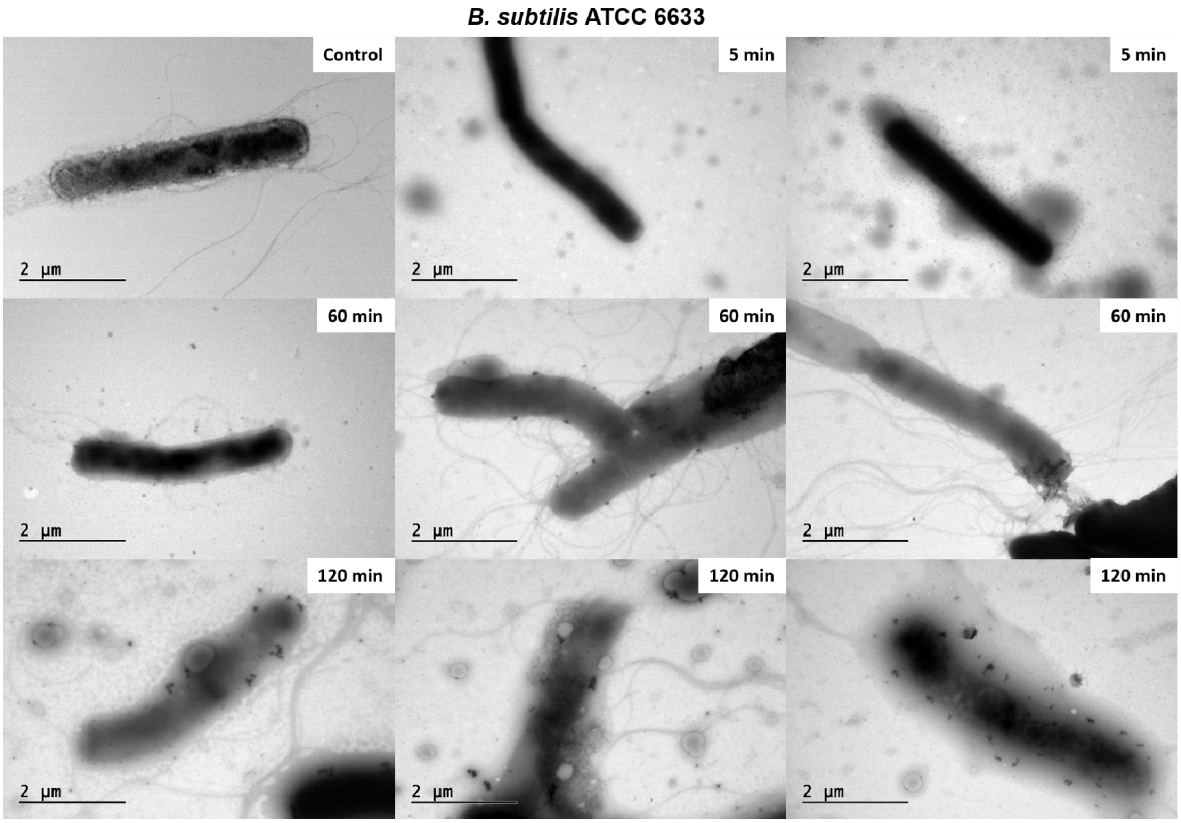

Figure S16. Additional TEM images of *B. subtilis* ATCC 6633 with TC_{NPs} over time.